Soft Matter

View Online
Dynamic Article Links

Cite this: *Soft Matter*, 2011, **7**, 6598

www.rsc.org/softmatter

PAPER

Interlayer distance dependence of thickness fluctuations in a swollen lamellar phase

Michihiro Nagao,*[ab] Sukhum Chawang[c] and Takumi Hawa[c]

Received 18th March 2011, Accepted 6th May 2011
DOI: 10.1039/c1sm05477e

Thickness fluctuations in a swollen lamellar structure, composed of a non-ionic surfactant, water and oil have been characterized by means of small-angle neutron scattering (SANS) and neutron spin echo (NSE) experiments, and coarse-grained molecular dynamics (CGMD) simulation. The static and dynamic structures of the membranes are measured as a function of the interlayer distance (membrane thickness), d_m. The oil to surfactant volume ratio is changed at a constant surfactant volume fraction, so that d_m is changed while maintaining the inter-lamellar repeat distance constant in the experiments. Two relaxation modes are observed from the NSE data, which are the bending motion and the thickness fluctuations. The bending rigidity of the membranes is a function of the membrane thickness. At low d_m the membranes become rigid due to the enhancement of the thickness fluctuations, while at large d_m the membranes tend to be flexible because of the decrease in the synchronization between the two interface layers. The thickness fluctuations are measured by NSE as an excess dynamics from the bending motion around the length scales of the membrane thickness, and a similar excess dynamics is observed in the CGMD simulation. Moreover, a method to estimate the thickness fluctuation amplitude in the experiment is proposed, and the validity of the method is verified by the simulation. An excellent agreement between the experiments and the simulations shows that the amplitude is about 12% of the membrane thickness and almost linearly increases with d_m. The present result shows the importance of the intra-membrane dynamics to determine the elastic properties of membranes, and the feasibility of the measurement of thickness fluctuations in surfactant membranes using NSE experiments and MD simulations.

Introduction

Surfactants are one of the basic building blocks of nano-scale self-assembling structures, such as micelles, microemulsion, and biological membranes. In particular, surfactant membranes play important roles from household and pharmaceutical products such as detergents, cosmetics, drugs, or foods to industrial applications such as oil recovery plants or the manufactures of nonstick surfaces. Production of the desired functionality, such as a reactivity with a particular molecules, and desired structure is seen as one of the major challenges in robust implementation of nanoscience to a nanotechnology. Furthermore, biological membranes, whose main components are various types of lipid molecules, are known as a platform for various biological functions. Interaction between lipid molecules and additives, such as sterol, drugs, and proteins, affects membrane dynamics. A wide variety of studies have been performed to elucidate the physical characteristics of model biomembranes. Understanding the behaviors of surfactant membranes and their properties is thus of both fundamental and industrial relevance.

One of the unique features of the membranes is thermally activated collective dynamics of surfactant molecules around room temperature. A membrane bending motion has been established both theoretically and experimentally.[1–13] Collective membrane fluctuations around the length scales of the membrane thickness have been probed by neutron spin echo (NSE) spectroscopy.[14–16] In Nagao's earlier paper,[16] different membrane dynamics were observed at the different length scales, which shed light on the localized membrane fluctuations. The following features were described: (i) the bending motion of bilayers was observed at length scales longer than the membrane thickness. (ii) Around the length scale corresponding to the membrane thickness, an excess dynamics in addition to the bending motion was observed and was interpreted as thickness fluctuations. (iii) At length scales smaller than the membrane thickness, a possibility of other intra-membrane movements was suggested.

[a]*NIST Center for Neutron Research, National Institute of Standards and Technology, Gaithersburg, MD, 20899-6102, USA. E-mail: mnagao@indiana.edu*
[b]*Center for Exploration of Energy and Matter, Indiana University, Bloomington, IN, 47408-1398, USA*
[c]*School of Aerospace and Mechanical Engineering, The University of Oklahoma, Norman, OK, 73019, USA*

The first investigation of thickness fluctuations examined dynamics in soap films. The fluctuations play an important role during the rupturing process.[17] In the 1980's, thickness fluctuations in a solvent free lipid bilayer were reported under equilibrium conditions based on laser light reflection results,[18–20] and Miller concluded that there is no energy change due to the fluctuations in bilayer membranes.[20] Haskell *et al.* studied thickness fluctuations in thin lipid films using reflectance fluctuation spectroscopy.[21] They concluded that the deduced values for the film viscosity and thickness compressibility were reasonable. Huang proposed a theory for lipid bilayer membranes based on deformation free energy.[22] For small deformations, the free energy consists of a layer-compression term, a splay-distortion term, and a surface tension term, which is equivalent to the elastic free energy of a two-layer smectic liquid crystal with surface tension. The thickness fluctuation amplitude for glyceryl monooleate-squalene membranes calculated from the theory was several tenths of nanometres.[22]

On the other hand, fluctuations on the scale of several nanoseconds, and spectral decomposition of both undulatory and thickness fluctuations in lipid bilayers were observed by molecular dynamics (MD) simulations.[23] The strength of membranes was also investigated in the same work. Inclusion of non-ionic surfactant considerably reduced both the extensibility and maximum stress that the bilayer can withstand.[24] The bending modulus of membranes was calculated by analyzing the undulation spectrum, and the effect of surfactant structure and composition of the monolayer on the bending modulus were investigated.[25] The bending modulus increases with chain length and is larger for linear surfactants than for branched ones. Recently, Shkulipa *et al.* used coarse-grained MD (CGMD) simulations to investigate the thermal undulations in lipid bilayers.[26] They observed a double exponential decay in their time correlations, with relaxation rates in good agreement with the model for bending and a slow mode originating from the density difference between two monolayers damped by the inter monolayer friction.[27] More recently, Brandt and Edholm investigated the stretched exponential dynamics in lipid bilayer simulations. Their MD results were not consistent with NSE data at low wave vectors.[28]

This review of previous experimental studies and numerical simulations indicates that membrane dynamics have been attracted by many researchers in the last four decades. However, thickness fluctuations observed by NSE[16] cannot be explained within the current theoretical framework. Therefore, further investigations in membrane dynamics are necessary for both fundamental and industrial relevance. So far, most of the experiments investigating thickness fluctuations employed visible light. Because of the wavelength involved (several hundreds nm), however, it is not easy to access dynamics in nm scale structures. Neutron scattering techniques, on the other hand, are powerful tools for investigating structure and dynamics on nm length scales. Cold neutrons have a wavelength around one nm with an energy of approximately 0.8 meV, which are suitable to investigating nm structures and their dynamics. Small-angle neutron scattering (SANS) gives structural information on length scales ranging from several nm to hundreds of nm, while the NSE technique provides dynamical information in the ns time range at those same length scales. So far, NSE has been used to discuss bending motion of membranes. Numerical simulation studies have extensively investigated bilayer or monolayer structures and their dynamics by calculating their bending modulus, or by taking self-correlation of the bilayer as the time correlation. However, to the best of our knowledge, collective dynamics of surfactant layers have never been investigated by combining numerical calculations and experiments.

In this paper, NSE and MD observations of thickness fluctuations as a function of interlayer distance (membrane thickness) in a swollen lamellar phase are reported, where the interlayer distance is controlled by the amount of oil. The dynamic range covered by NSE and MD, in nm and ns ranges, is more appropriate for membrane dynamics, especially thickness fluctuations. In MD simulations, periodic boundary conditions are used to mimic a large system, and samples are equilibrated in the simulation system. In NSE, on the other hand, no restriction of sample geometry is required, thus studies are possible in natural environments, namely in dispersions. The static structure of the system was also investigated by SANS and MD.

Experiments

The measured system was a ternary mixture of pentaethylene glycol dodecyl ether ($C_{12}E_5$), deuterium oxide (D_2O), and deuterated octane (C_8D_{18}). This system shows a variety of self-assembled structures depending on composition, temperature, and so on.[29,30] The ratio between the volume fraction of oil ϕ_o and that of surfactant ϕ_s, $R = \phi_o/\phi_s$, was varied to control the membrane thickness, where the membrane consists of an oil layer sandwiched by two surfactant monolayers. This system exhibits a lamellar phase in the water rich corner and has been thoroughly investigated by Kahlweit *et al.*[31] With fixing ϕ_s, lamellar structure is known to appear at $T \approx 30$ °C with changing oil to water volume ratio. Only at $R = 0$, corresponding to pure bilayers of $C_{12}E_5$ in water, it is known the lamellar structure appears at higher temperature. All the experimental data shown in this paper were measured in an isotropic lamellar phase.[30,32] In order to keep the mean repeat distance of the lamellae constant while adjusting the membrane thickness as illustrated in Fig. 1, R was varied from 0 to 2 while keeping $\phi_s = 0.041$.

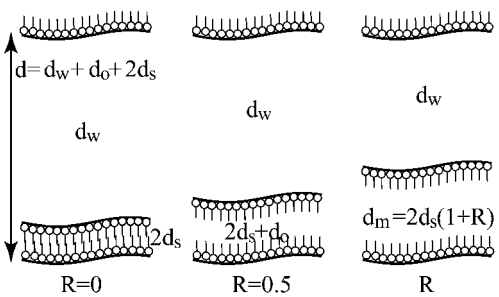

Fig. 1 A schematic illustration of the present system. Addition of oil to the system swells the $C_{12}E_5$ bilayers. Since the volume fraction of surfactant is kept constant, the inter lamellar distance, d, is constant, while the bilayer thickness, $d_m = 2d_s + d_o = 2d_s\,(1 + R)$, increases with increasing R, where d_s and d_o are the surfactant molecular length and the oil layer thickness. $R = 0$ corresponds to the case of pure bilayers.

The SANS experiments were conducted on the NG3- and NG7-SANS instruments at the National Institute of Standards and Technology (NIST) Center for Neutron Research (NCNR), USA[33,34] to verify the R-dependence of the structure change of the system. The incident neutron wavelengths, λs, were selected to be 0.6 nm and 0.806 nm for the NG3 and NG7, respectively, with their resolution of about 11%. The incident neutron beam was irradiated to samples and scattered neutrons were detected by a two-dimensional position sensitive detector. The momentum transfer q ($=4\pi\lambda^{-1}\sin\theta$; 2θ is the scattering angle) ranged from 0.01 nm^{-1} to 3.7 nm^{-1}, which corresponds to length scales from 0.3 nm to 100 nm. Temperature was controlled using a water circulation bath system at $T = (31.6 \pm 0.1)$ °C for $0.2 \leq R \leq 2$. $R = (0$ and $0.1)$ samples were measured at $T = (59.6 \pm 0.2)$ °C. The observed two dimensional data were azimuthally averaged and normalized to an absolute intensity using the SANS data reduction program developed at NIST.[35]

The NSE experiments were conducted on the NG5-NSE[36,37] at the NCNR and iNSE[38,39] of the Univ. of Tokyo, Japan. The 0.6 nm and 0.8 nm incident neutron beams were mechanically selected with a wavelength resolution of about 20% for NG5-NSE. A 0.7 nm neutrons with a spread of about 15% were used at iNSE. Larmor precession angles of polarized neutron spins were used to measure the energy transfer within samples. The q and time t ranges covered were $0.4\ nm^{-1} \leq q \leq 2.1\ nm^{-1}$ and $0.05\ ns \leq t \leq 40$ ns at NG5-NSE and $0.3\ nm^{-1} \leq q \leq 1.6\ nm^{-1}$ and $0.1\ ns \leq t \leq 15$ ns at iNSE. The sample compositions were $\phi_s = 0.041$ and $R = 0$, 0.3, 0.5, 1.0, and 1.37. The sample thickness was selected to be 2 mm. The temperature was controlled at (30 ± 0.1) °C except for the sample of $R = 0$ which was measured at $T = (55.0 \pm 0.1)$ °C. Water circulation systems were used for the temperature control. The DAVE software package was used for the data reduction of the NG5-NSE data.[40] Note that although the measured temperatures were slightly different between the SANS and NSE experiments, no difference was seen in the SANS profiles.

Simulations

The above ternary system (non-ionic surfactants in oil and water) is modeled by the MARTINI course-grained (CG) force field, version 2.0,[41] which is widely used to study the dynamics of monolayer or bilayer membranes in water and oil. In the MARTINI force field, polar, apolar, and nonpolar beads are denoted as head (H), tail (T), and nonpolar (N), respectively. A water bead represents a group of four water molecules, an oil molecule consists of two tail beads, and a surfactant molecule is modeled as one head bead and two nonpolar plus two tail beads physically connected to each other. The interactions of CG sites are described by the Lennard-Jones and Coulomb potentials. Bonded interactions between the chemically connected sites are described by harmonic stretching and bending potentials. Details of the model equations and parameters are described by Marrink *et al.*[42] for water and oil and by Sanders and Panagiotopoulos for surfactants.[43] The number of water, oil, and surfactant beads is 40 000, 15 000, and 6000 for $R = 0.57$ in a $15.6 \times 22.5 \times 22.5\ nm^3$ simulation box with periodic boundary conditions in all directions. Simulations are performed by Gromacs package Version 4[44] with an integration time step of 25 fs, and the Berendsen thermostat and barostat schemes on Dell Precision T7500 workstations, which have Dual Six Core Intel Xeon Processor X5680, 3.33 GHz each, in Hawa Lab at the University of Oklahoma. The simulations were run for 200 ns at 30 °C and at 1 bar to equilibrate the system and for 50 ns to calculate the intermediate scattering function, $I(q,t)$, as

$$I(q,t) = \frac{1}{N}\sum_{i=1}^{N}\sum_{j=1}^{N}\left\langle \exp\left[iq\{r_i(t) - r_j(0)\}\right]\right\rangle \quad (1)$$

where q is a momentum transfer vector, r_i is a position vector for particle i, t is a time, and N is the number of third (center) beads of surfactant molecules. Note that we only chose the center beads of surfactants for calculating $I(q,t)$ to maximize the computational efficiency. This choice of computation induces a clear distinction between the surfactant layers even at $R = 0$. The measured sample compositions were $\phi_s = (0.06$ to $0.07)$ and $R = (0, 0.31, 0.57, 0.88,$ and $1.14)$, and q ranges were from $0.5\ nm^{-1}$ to $2.5\ nm^{-1}$. For each calculation of $I(q,t)$ we averaged over 150 sampling time with 360 directions of q. In general (experiments) the averaged angle of the sampling directions is approximately 33 degree from the surface of the membrane, while we chose it to be approximately 45 degree to observe clearer peak profiles originating from the form factor of the membranes in the high-q region.

Results and discussion

A typical SANS profile from an isotropic lamellar structure with varying R is shown in Fig. 2(a). In the low-q region, a broad scattering peak, which originates from the Bragg reflection of the membrane stacking, is observed around $q = 0.08\ nm^{-1}$ for large R. Although the peak position of the lamellae is not clear for samples at $R \leq 1.2$, the peak position is considered to be almost independent of R since the peak positions are coincident to each other at $R = 1.5$ and 2.0. On the other hand, in the high-q region, a clear peak profile originating from the form factor of the membranes is observed. With increasing R, the characteristic q value, which is the dip and/or peak position of the form factor, shifts toward lower q. A constant inter-lamellar distance with changing membrane thickness as illustrated in Fig. 1 is confirmed from the SANS profiles.

Fig. 2(b) shows the intermediate scattering function at time $t = 0$, $I(q,t = 0)$, obtained from the MD simulation. This profile corresponds to the SANS profiles observed in the experiment. The $I(q,t = 0)$ is calculated at $T = 30$ °C. A much clearer peak profile originating from the form factor of the membranes is observed in the high-q region. This is due to the choice of our sampling direction of q vectors and the position of the sampling beads of surfactants. The characteristic q value shifts toward lower q with increasing R, which agrees with experimental observations. This confirms the capability of comparison of our experimental data to the data obtained in the MD simulations. Note that the $I(q,t = 0)$ at low-q does not reproduce the SANS profiles well. This might be due to the limited simulation size. The structure and, thus, dynamics at the length scales of inter-lamellar spacing are not well reproduced in the present MD simulations.

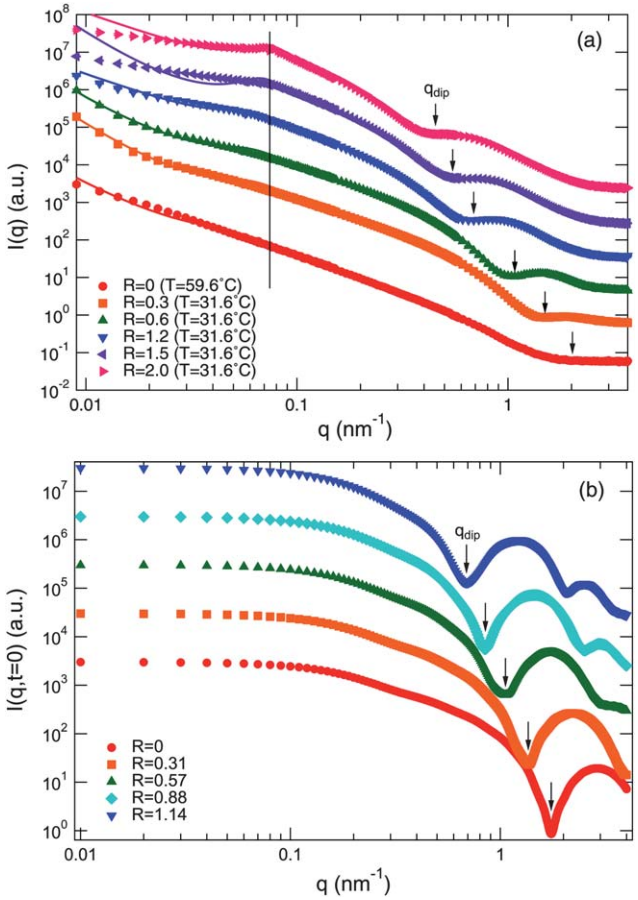

Fig. 2 (a) Typical SANS profiles obtained from a lamellar structure consisting of $C_{12}E_5$, D_2O, and C_8D_{18} at $T = 31.6$ °C except for $R = 0$, which was measured at $T = 59.6$ °C. Lines are fits to the data according the Lemmich model.[45] Error bars, shown as a ±1 standard deviation throughout this paper, are smaller than the symbols. (b) Corresponding q dependence of $I(q,t = 0)$ from MD simulations for various R at $T = 30$ °C. The arrows indicate the positions of q_{dip} estimated taking derivative of the SANS and $I(q,t = 0)$ curves.

The SANS profiles are analyzed utilizing a model scattering function proposed by Lemmich *et al.*[45] Although the Lemmich model was proposed to explain multilamellar peak profile in lipid bilayers, the theory is applicable to the scattering profiles from the powder averaged (isotropic) lamellar structures in ternary microemulsion systems. The scattering length densities of the head, ρ_h, and tail, ρ_t, of a lipid in the original model are replaced with those of surfactant, ρ_s, and oil, ρ_o, respectively. In their model, the scattering intensity from the lamellar structure was calculated on the basis of the paracrystalline theorem. The model scattering function and the detail of the theory are described in their original paper.[45]

The solid lines in Fig. 2(a) are the fit results to the model. The ideal swelling law of the lamellar structure is assumed to perform the fit. The relations are the oil layer thickness $d_o = 2Rd_s$, the water layer thickness $d_w = 2d_s\{\phi_s^{-1} - (1 + R)\}$, the mean repeat distance of lamellae $d = d_w + d_o + 2d_s = 2d_s\phi_s^{-1}$, and the membrane thickness $d_m = d_o + 2d_s = 2d_s(1 + R)$, where d_s is the surfactant layer thickness. The R dependence of d_m is shown in Fig. 3. The solid straight line shows the result of a linear fit to the ideal swelling law and $d_s = (1.55 \pm 0.01)$ nm is obtained from the slope, which is close to the value in the literature.[30]

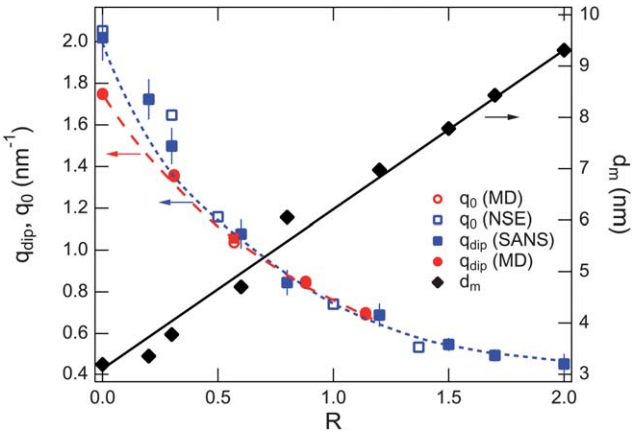

Fig. 3 R dependence of the membrane thickness d_m (full diamonds), the dip position q_{dip} in SANS (full squares) and in MD (full circles), and the peak position q_0 in Γ/q^3 observed by NSE (open squares) and by MD (open circles). d_m is shown on the right axis and the solid straight line indicates a linear fit to the ideal swelling law. q_{dip} and q_0 are shown on the left axis. The dashed lines are guides for the eyes.

Fig. 4(a) shows a normalized intermediate scattering function, $I(q,t)/I(q,0)$, observed by NSE at $R = 0.3$ and $T = 30$ °C. As explained in the previous paper, $I(q,t)/I(q,0)$ follows a stretched exponential behavior with the stretching exponent $\beta = 2/3$.[16] This

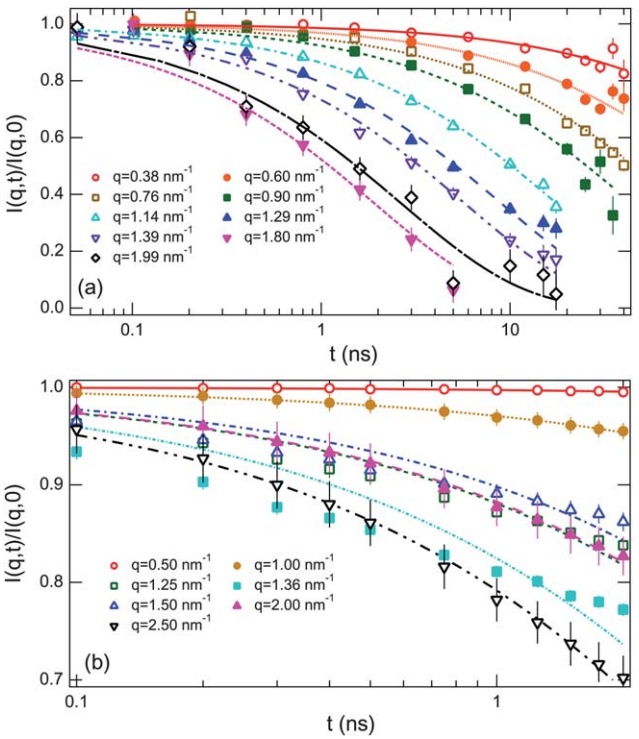

Fig. 4 (a) Observed normalized intermediate scattering function, $I(q,t)/I(q,0)$, from $R = 0.3$ at $T = 30$ °C. The lines are the fits to the data according to eqn (2). (b) Corresponding $I(q,t)/I(q,0)$ from MD simulations for $R = 0.31$ at $T = 30$ °C.

trend is confirmed for various R. The lines in Fig. 4(a) are the fit results according to the following relation,

$$\frac{I(q,t)}{I(q,0)} = \exp\left[-(\Gamma t)^{2/3}\right] \quad (2)$$

The lines obtained from the MD simulations also decay with time and the decay rates increase with q values as shown in Fig. 4(b). In the intermediate q-range the decay rates do not follow the same order in q. This originates from the contribution from a faster dynamics, which is the subject of this paper. The decay function is also well explained with eqn (2) except for the intermediate q range, ex., $q = 1.36$ nm^{-1} in Fig. 4(b). This result suggests that the thickness fluctuations can be expressed as faster dynamic mode, and in the intermediate q-range, multiple exponential functions might be better for the analyses. In the present paper, however, we do not go into detail about this point, which is a future problem.

The observed relaxation rates Γ in the experiments and the simulations are shown in Fig. 5(a) and (c). They show two components in the dynamics: One is proportional to q^3 indicating the bending motion, and the other is an excess (faster) motion in a finite range of q. The q range for the appearance of the excess mode depends on R. Eqn (2) has been proposed by Zilman and Granek[6] as the theory to explain the thermal undulations of a thin elastic sheet based on the Helfrich bending Hamiltonian.[1] In their model, the decay rate Γ is proportional to q^3 in the range $1/d < q < 1/d_m$. Thus, this model should explain the present data in the low-q region. The other component is observed at the q close to the dip position in the SANS profile, which corresponds to the length scale of the membrane thickness ($qd_m \approx 6$). Fig. 5 (a) and (c) show that the decay rates in MD are about three orders of magnitude slower than those of the NSE. This implies that the membrane in MD is stiffer than that measured by NSE. There might be two possible causes for this. The first possibility is that it stems from our choice of potential, and the second possibility is that it stems from the finite size of the computational domain unit ($15.6 \times 22.5 \times 22.5$ nm^3 for $R = 0.57$), which is much smaller than that covered by experiments. This might cause a deviation from the q^3 relation of Γ at low q shown in Fig. 5(c). Even thought the periodic boundary conditions are introduced in MD, the computational unit domain may limit the bending motion of the membrane while it should not limit the excess fluctuations of the membrane. Thus, the $I(q,t)/I(q,0)$ observed in MD decays too slowly to estimate the decay rates especially for the low q values, while the enhanced motion is observed well. In the remainder of this paper, we do not show the results for the bending dynamics observed in the MD simulation.

Fig. 5(b) and (d) present the q-dependence of Γ/q^3 for various R of the experiments and simulations. A difference in the peak position in Γ/q^3 for $R = (0$ and $0.3)$ is clearly visible here. The reason for this difference will be discussed later. With increasing R, the peak position in Γ/q^3 shifts to lower q in both figures. This is consistent with the shift of the form factor scattering to lower q observed by SANS and MD (see Fig. 2). To characterize the dynamic behavior, a Lorentz function is utilized to fit the q dependence of Γ/q^3 following the previous procedure.[16] In this procedure, two terms are considered as membrane dynamics in the observed decay rate. One is the contribution from the

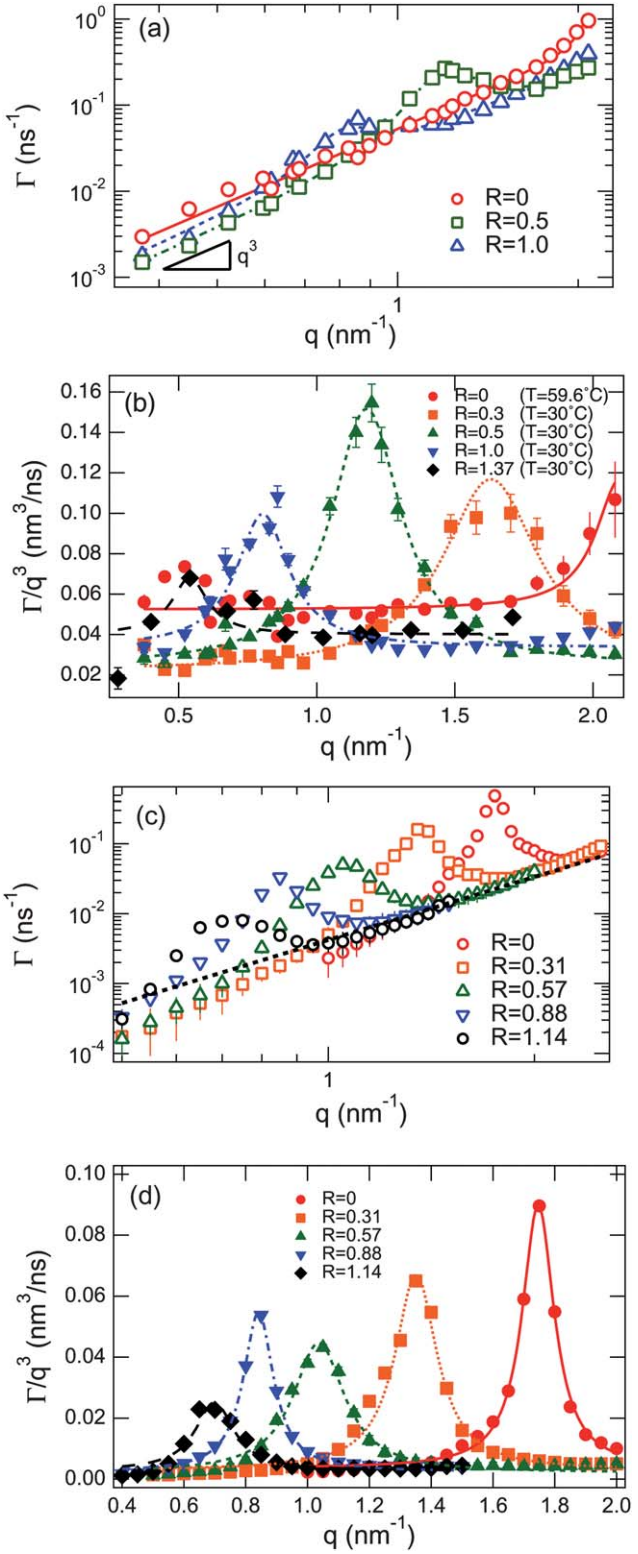

Fig. 5 (a) q Dependence of Γ observed by NSE. The solid straight line shows the theoretical prediction by the Zilman and Granek model,[6] $\Gamma \propto q^3$. The dashed curves are guides for the eyes. (b) q dependence of Γ/q^3 obtained from NSE results. The lines are fit results according to eqn (3). (c) q dependence of Γ and (d) q dependence of Γ/q^3 from MD simulations for various R. The dashed line in (c) is a guide for the eyes. The curves in (d) are the results of fitting to eqn (3).

bending motion, characterized by a decay rate Γ_{ZG}, and the other is from the thickness fluctuations, characterized by Γ_{TF}. The lines in Fig. 5(b) and (d) are fit results to the following equation,

$$\frac{\Gamma}{q^3} = \frac{\Gamma_{TF}}{q_0^3}\frac{1}{1+(q-q_0)^2\xi^{-2}} + \frac{\Gamma_{ZG}}{q^3} \quad (3)$$

where Γ_{TF}/q_0^3 is the peak height, q_0 the peak position, ξ^{-1} is the half-width at half maximum of the peak, and Γ_{ZG}/q^3 the base line for the Lorentz function, respectively. This treatment is useful in order to emphasize the deviation of the thickness fluctuations from the bending motion. The first term originates from the thickness fluctuations of the membrane, and the second term from the single membrane undulation. As defined in the previous paper,[16] each parameter relates to that of the thickness fluctuations as: Γ_{TF}/q_0^3 and ξ^{-1} are proportional to the damping frequency of the mode and the mode amplitude, and q_0 is the center of the motion, which relates to the membrane thickness, respectively. It is noted that even for the $R = 0$ sample, corresponding to the pure bilayers, the thickness fluctuations are observed (see Fig. 5). On the other hand, the $R = 1.37$ (NSE data in Fig. 5(b)) and $R = 1.14$ (MD data in Fig. 5(d)) samples show a small enhancement of the dynamics. This suggests that large amount of oil, which swells the bilayers, suppresses the thickness fluctuations.

The comparison between the dip positions in SANS and MD, q_{dip}, and the peak position in NSE and MD, q_0, are shown in Fig. 3. The q_{dip} was estimated by taking derivative of the SANS profiles and $I(q,t = 0)$ in the experiments and simulations, respectively. The q_{dip} and q_0 are almost coincident in both the experiments or the MD, indicating the peak-like behavior in Γ originates from the motion near the length scales of the membrane thickness. However, a deviation between experiments and simulations appears at low R especially at $R \leq 0.3$. The scattering contrast dependence of the thickness fluctuations shows a larger value of q_{dip} or q_0 for the bulk contrast samples in which C_8D_{18} is replaced by C_8H_{18} at the same volume fraction of the sample.[46] At $R = 0$ hydrogenated surfactants form bilayers, which are seen as one single layer by neutrons. On the other hand, for $R = 0.3$ the shift of q_{dip} from the film contrast to the bulk contrast was confirmed by another SANS measurement (data not shown). In the MD simulations, correlations among the center (third) beads of the surfactant molecules are taken for the calculations. This condition is the same as the film contrast for the experiment. Thus, the R dependence of q_{dip} and q_0 from the MD calculations is for the film contrast sample. This contrast dependence is a likely cause for the high q shift of the q_{dip} and q_0 at $R \leq 0.3$. However, only from the scattering contrast, $R = 0.3$ data cannot be explained, and thus this point remains for future studies.

Fig. 6 shows a distribution of local fluctuations of surfactants from the average membrane thickness for $R = 0.57$ in the MD simulations. This histogram sampled from 400 local regions in the computational domain for every 50 ps over 15 ns for each membrane thickness. This histogram is approximated by a Gaussian distribution, and its standard deviation, σ, estimates the local fluctuation as 0.58 nm. We also project the local distribution of surfactants from the width of the peak ξ^{-1} for each membrane thickness in Fig. 5(d). The ratio ξ^{-1}/q_0 indicates the

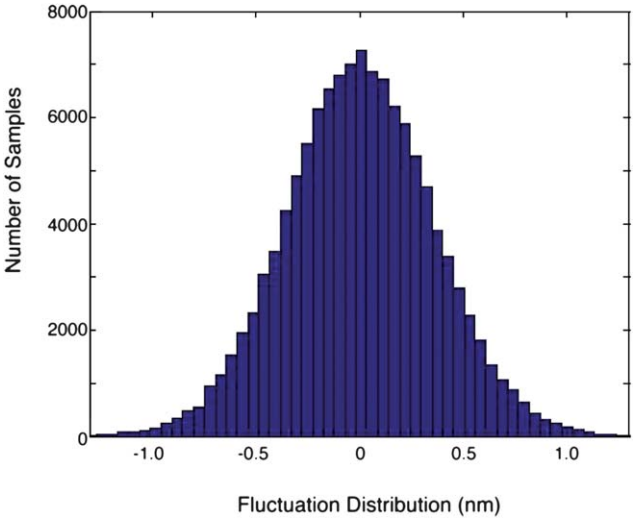

Fig. 6 Distribution of thicknesses around the average membrane thickness for $R = 0.57$ in MD simulations.

fraction of the thickness fluctuation amplitude. Thus, $d_m\xi^{-1}/q_0$ corresponds to the actual amplitude of the thickness fluctuations. The value of $d_m\xi^{-1}/q_0 \approx 0.43$ nm is estimated for $R = 0.57$ in the MD simulation, which is reasonably well coincident to the value of σ. This result suggests that the width parameter in Γ/q^3 directly relates to the thickness fluctuation amplitude.

The standard deviations, σ, in real space and $d_m\xi^{-1}/q_0$ in Fourier space for all membrane thicknesses, R, are summarized in Fig. 7. The values of σ are slightly larger than those of $d_m\xi^{-1}/q_0$ for all thicknesses in the MD simulations. Note that the deviation of the results between σ and $d_m\xi^{-1}/q_0$ for $R = 0.88$ is large because of the high peak of the excess dynamics observed in Fig. 5(d). These good agreements for the various values of R suggest that the distribution of the thickness fluctuations can be estimated from the width of the peak of Γ/q^3 in Fourier space, which thus provides a method to estimate the thickness fluctuation amplitude from experimental measurements.

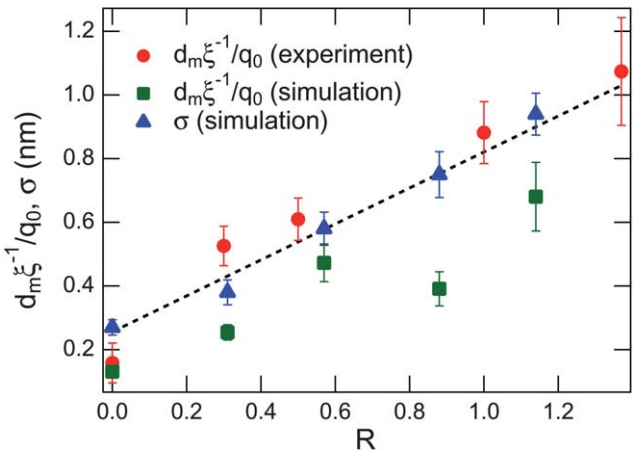

Fig. 7 Standard deviations, σ, in real space and $d_m\xi^{-1}/q_0$ in Fourier space from simulations and $d_m\xi^{-1}/q_0$ from experiments as a function of membrane thicknesses, R.

As shown in Fig. 7, the experimentally observed value of $d_m\xi^{-1}/q_0$ is larger than that from the simulation except for $R = 0$. The estimation of ξ^{-1} and q_0 for $R = 0$ from the experiment is quite poor because of the accessible q-range. However, the agreement between the experimental $d_m\xi^{-1}/q_0$ and σ is excellent. This estimate indicates that the observed motion in the NSE experiment is the thickness fluctuations in surfactant membranes, and that the thickness fluctuation amplitude linearly increases with the membrane thickness. The fraction of the thickness fluctuation amplitude is almost constant with R at about 12% of the membrane thickness.

The bending motion of the membranes is characterized by Γ_{ZG} in eqn (3). As predicted by Zilman and Granek, Γ_{ZG} relates to the bending modulus, κ, as follows,[6]

$$\Gamma_{ZG} = 0.025\gamma(k_BT)^{3/2}k^{-1/2}\eta^{-1}q^3 \quad (4)$$

where γ originates from averaging over the angle between the wave vector and the plaquette surface normal in the calculation of $I(q,t)/I(q,0)$, and k_B, T, and η are Boltzmann's constant, the absolute temperature, and the viscosity of the solvent, respectively. Utilizing the above equation, the R dependence of κ was estimated as shown in Fig. 8. As in the previous treatment,[16] we put $\gamma = 1$ and the value of $3\eta_{D2O}$ as the effective viscosity instead of the viscosity of D_2O, η_{D_2O}, in order to account for the local energy dissipation.[9] The physical meaning of the factor of three has recently been described in the literature.[47,48]

The κ at $R = 0.3$ is larger than that of the pure bilayers ($R = 0$). This means that the membranes are more rigid around $R = 0.3$ than the pure bilayers. Two possible scenarios are considered. One is the increase of κ due to the change in the bilayer thickness. The other scenario is that the increase in κ originates from the lateral mobility of the oil molecules within the membranes. This makes it possible to dissipate energy within the membrane as the thickness fluctuations. In this case the bending motion of bilayers is effectively suppressed due to the enhanced thickness fluctuations, and the apparent bending modulus could be larger than that of the pure bilayers. In other words, the surfactant bilayers are not required to highly bend to dissipate energy to the surrounding medium, because the thickness fluctuations help to dissipate energy within the membranes.

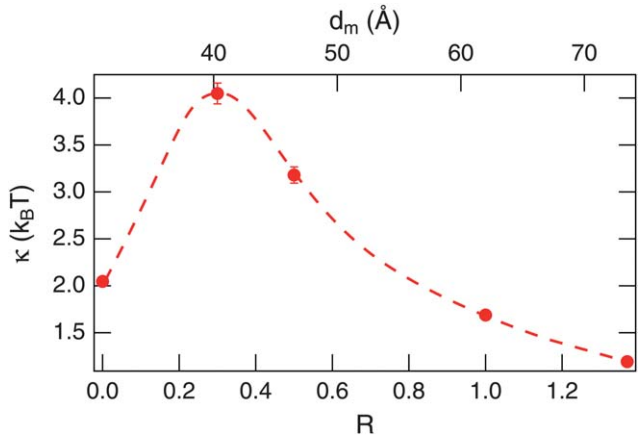

Fig. 8 R dependence of κ obtained by NSE. The dashed line is a guide for the eyes. In the low swelling condition, κ has a maximum at $R = 0.3$. Above $R = 0.3$ κ decreases with R. At $R = 1.37$ the value of κ is almost 1 k_BT, which is close to the bending modulus of monolayers of $C_{12}E_5$.

With increasing R the value of κ becomes smaller at $R > 0.3$, and finally at $R = 1.37$ κ is about 1 k_BT, which is close to the literature value for $C_{12}E_5$ monolayers.[7] This result is consistent with the membrane thickness dependence of κ in the literature.[49,50] According to Kurtisovski *et al.*,[50] a decrease of the bending rigidity is observed when increasing the water thickness. In their case two surfactant monolayers sandwich a water layer. They suggested that when the water thickness is small enough, the fluctuations of the two monolayers are synchronized: the two monolayers act as a single thick membrane. The two monolayers start to be less coupled and will fluctuate independently for larger water content.[50] The R dependence of κ in the present result can be explained with the same concept. Therefore, above $R = 1.37$ it is possible to treat the surfactant membranes as monolayers, while below $R = 1.37$ the membranes should be treated like bilayers in some way. The decrease in κ at large R originates from the decrease in synchronization between monolayers.

The present result indicates the importance of intra-membrane dynamics to the elastic properties of the overall membrane. The rigidity of membranes is determined not only by the interactions among molecules but also by the energy dissipation mechanisms within the membranes. Although a compression mode is a candidate dissipation mechanism within the membrane,[27,51] this mode is observed as a slower motion than the bending,[51] which suggests that different mechanisms from the compression mode also contribute to the intra-membrane dynamics. Moreover, the present results, as well as the methods described here, might be very useful to understanding the dynamics of surfactant membranes and their properties, in particular, in the fields of bilayer lipid membranes, interaction of drugs with biomembranes, and transportation of molecules across the skin and its protection.

Conclusion

In this paper, the interlayer distance dependence of the thickness fluctuations was examined in the swollen lamellar phase composed of water, $C_{12}E_5$, and octane by SANS and NSE experiments and MD simulations. The oil layer is sandwiched by surfactant monolayers and the amount of oil is controlled to vary the interlayer distance (membrane thickness), as confirmed by SANS and MD data. The dynamics of the membrane were measured by NSE and MD and two relaxation modes were detected. The first mode is the well-known bending motion, which depends on the membrane thickness. The other one is an intra-membrane motion identified as thickness fluctuations. The thickness fluctuations are observed over a range of interlayer distances from 3 nm to 7 nm. The thickness fluctuation amplitude was estimated from the simulation both in real and Fourier space, and from the experiment. An excellent agreement between experimental and simulation parameters supports the idea that the excess dynamics measured by NSE is due to thickness fluctuations and that the estimated thickness fluctuation amplitude is reasonable. The membrane rigidity is a function of the membrane thickness. At low thickness conditions the membranes become rigid due to the enhancement of the thickness fluctuations, while at high thickness conditions the membranes

become flexible due to the decrease in synchronization between the two interface layers. The lateral mobility of the oil molecules helps the thickness fluctuations in the low swelling regime, while bending fluctuations of individual surfactant monolayers become dominant in the high swelling regime. The present results indicate that the intra-membrane fluctuations are important in determining the elastic property of the membrane. The combined use of NSE and MD, which verified the thickness fluctuations of the membranes in this paper, emerges as powerful tools to describe localized collective dynamics of membranes.

Disclaimer

Certain commercial products, softwares, or materials are identified in this paper to foster understanding. Such identification does not imply recommendation or endorsement by the National Institute of Standards and Technology, nor does it imply that the software or materials identified are necessarily the best available for the purpose.

Acknowledgements

MN acknowledges Drs P. Butler and S. R. Kline for their help to perform SANS experiment and Prof. H. Seto, Drs A. Faraone and D. Neumann for many helpful discussion. This work utilized facilities supported in part by the National Science Foundation under Agreement No. DMR-0944772.

References

1 W. Helfrich, *Z. Naturforsch., C: Biochem., Biophys., Biol., Virol.*, 1973, **28**, 693.
2 S. T. Milner and S. A. Safran, *Phys. Rev. A: At., Mol., Opt. Phys.*, 1987, **36**, 4371.
3 J. S. Huang, S. T. Milner, B. Farago and D. Richter, *Phys. Rev. Lett.*, 1987, **59**, 2600.
4 B. Farago, D. Richter, J. S. Huang, S. A. Safran and S. T. Milner, *Phys. Rev. Lett.*, 1990, **65**, 3348.
5 S. A. Safran, *Statistical Thermodynamics of Surfaces, Interfaces and Membranes*, Westview Press, Boulder, CO, 1994.
6 A. G. Zilman and R. Granek, *Phys. Rev. Lett.*, 1996, **77**, 4788.
7 T. Hellweg and D. Langevin, *Phys. Rev. E: Stat. Phys., Plasmas, Fluids, Relat. Interdiscip. Top.*, 1998, **57**, 6825.
8 C. H. Lee, W. C. Lin and J. P. Wang, *Phys. Rev. E: Stat., Nonlinear, Soft Matter Phys.*, 2001, **64**, 020901(R).
9 S. Komura, T. Takeda, Y. Kawabata, S. K. Ghosh, H. Seto and M. Nagao, *Phys. Rev. E: Stat. Phys., Plasmas, Fluids, Relat. Interdiscip. Top.*, 2001, **63**, 041402.
10 M. Mihailescu, M. Monkenbusch, J. Allgaier, H. Frielinghaus, D. Richter, B. Jakobs and T. Sottmann, *Phys. Rev. E: Stat. Phys., Plasmas, Fluids, Relat. Interdiscip. Top.*, 2002, **66**, 041504.
11 M. Monkenbusch, O. Holderer, H. Frielinghaus, D. Byelov, J. Allgaier and D. Richter, *J. Phys.: Condens. Matter*, 2005, **17**, S2903.
12 M. Nagao and H. Seto, *Phys. Rev. E: Stat., Nonlinear, Soft Matter Phys.*, 2008, **78**, 011507.
13 Z. Yi, M. Nagao and D. P. Bossev, *J. Phys.: Condens. Matter*, 2009, **21**, 155104.
14 B. Farago, M. Monkenbusch, K. D. Goecking, D. Richter and J. S. Huang, *Phys. B*, 1995, **213**, 712.
15 B. Farago, *Phys. B*, 1996, **226**, 51.
16 M. Nagao, *Phys. Rev. E: Stat., Nonlinear, Soft Matter Phys.*, 2009, **80**, 031606.
17 A. Vrij, *Faraday Discuss. Chem. Soc.*, 1966, **42**, 23.
18 D. Bach and I. R. Miller, *Biophys. J.*, 1980, **29**, 183.
19 S. B. Hladky and D. W. R. Gruen, *Biophys. J.*, 1982, **38**, 251.
20 I. R. Miller, *Biophys. J.*, 1984, **45**, 643.
21 R. C. Haskell, D. C. Petersen and M. W. Johnson, *Phys. Rev. E: Stat. Phys., Plasmas, Fluids, Relat. Interdiscip. Top.*, 1993, **47**, 439.
22 H. W. Huang, *Biophys. J.*, 1986, **50**, 1061.
23 E. Lindahl and O. Edholm, *Biophys. J.*, 2000, **79**, 426.
24 R. D. Groot and K. L. Rabone, *Biophys. J.*, 2001, **81**, 725.
25 L. Rekvig, B. Hafskjold and B. Smit, *J. Chem. Phys.*, 2004, **120**, 4897.
26 S. A. Shkulipa, W. K. den Otter and W. J. Briels, *J. Chem. Phys.*, 2006, **125**, 234905.
27 U. Seifert and S. A. Langer, *Europhys. Lett.*, 1993, **23**, 71.
28 E. G. Brandt and O. Edholm, *J. Chem. Phys.*, 2010, **133**, 115101.
29 R. Strey, R. Schomacker, D. Roux, F. Nallet and U. Olsson, *J. Chem. Soc., Faraday Trans.*, 1990, **86**, 2253.
30 M. Nagao, H. Seto, D. Ihara, M. Shibayama and T. Takeda, *J. Chem. Phys.*, 2005, **123**, 054705.
31 M. Kahlweit, et al., *J. Colloid Interface Sci.*, 1987, **118**, 436.
32 M. Leaver, V. Rajagopalan, O. Ulf and K. Mortensen, *Phys. Chem. Chem. Phys.*, 2000, **2**, 2951.
33 C. J. Glinka, J. G. Barker, B. Hammouda, S. Krueger, J. J. Moyer and W. J. Orts, *J. Appl. Crystallogr.*, 1998, **31**, 430.
34 S. M. Choi, J. G. Barker, C. J. Glinka, Y. T. Cheng and P. L. Gammel, *J. Appl. Crystallogr.*, 2000, **33**, 793.
35 S. R. Kline, *J. Appl. Crystallogr.*, 2006, **39**, 895.
36 N. Rosov, S. Rathgeber and M. Monkenbusch, in *Scattering from Polymers—Characterization by X-Rays, Neutrons, and Light*, ed. P. Cebe, B. S. Hsiao and D. J. Lohse, American Chemical Society, Washington, 2000, vol. 739, p. 103.
37 M. Monkenbusch, R. Schatzler and D. Richter, *Nucl. Instrum. Methods Phys. Res., Sect. A*, 1997, **399**, 301.
38 T. Takeda, et al., *Nucl. Instrum. Methods Phys. Res., Sect. A*, 1995, **364**, 186.
39 M. Nagao, N. L. Yamada, Y. Kawabata, H. Seto, H. Yoshizawa and T. Takeda, *Phys. B*, 2006, **385–386**, 1118.
40 R. T. Azuah, L. R. Kneller, Y. M. Qiu, P. L. W. Tregenna-Piggott, C. M. Brown, J. R. D. Copley and R. M. Dimeo, *J. Res. Natl. Inst. Stand. Technol.*, 2009, **114**, 341.
41 S. J. Marrink, H. J. Risselada, S. Yefimov, D. P. Tieleman and A. H. de Vries, *J. Phys. Chem. B*, 2007, **111**, 7812.
42 S. J. Marrink, A. H. de Vries and A. E. Mark, *J. Phys. Chem. B*, 2004, **108**, 750.
43 S. A. Sanders and A. Z. Panagiotopoulos, *J. Chem. Phys.*, 2010, **132**, 114902.
44 D. Van der Spoel, E. Lindahl, B. Hess, G. Groenhof, A. E. Mark and H. J. C. Berendsen, *J. Comput. Chem.*, 2005, **26**, 1701.
45 J. Lemmich, K. Mortensen, J. H. Ipsen, T. Honger, R. Bauer and O. G. Mouritsen, *Phys. Rev. E: Stat. Phys., Plasmas, Fluids, Relat. Interdiscip. Top.*, 1996, **53**, 5169.
46 M. Nagao, submitted.
47 M. C. Watson and F. L. H. Brown, *Biophys. J.*, 2010, **98**, L9.
48 J. H. Lee, S. M. Choi, C. Doe, A. Faraone, P. A. Pincus and S. R. Kline, *Phys. Rev. Lett.*, 2010, **105**, 038101.
49 E. Freyssingeas, D. Roux and F. Nallet, *J. Phys.: Condens. Matter*, 1996, **8**, 2801.
50 E. Kurtisovski, N. Taulier, R. Ober, M. Waks and W. Urbach, *Phys. Rev. Lett.*, 2007, **98**, 258103.
51 L. R. Arriaga, R. Rodriguez-Garcia, I. Lopez-Montero, B. Farago, T. Hellweg and F. Monroy, *Eur. Phys. J. E*, 2010, **31**, 105.